HARP Collaboration

TPC cross-talk correction: CERN–Dubna–Milano algorithm and results

A. De Min, F. Dydak, A. Guskov, A. Krasnoperov, Yu. Nefedov, A. Zhemchugov

Abstract

The CDM (CERN-Dubna-Milano) algorithm for TPC Xtalk correction is presented and discussed in detail. It is a data-driven, model-independent approach to the problem of Xtalk correction. It accounts for arbitrary amplitudes and pulse shapes of signals, and corrects (almost) all generations of Xtalk, with a view to handling (almost) correctly even complex multi-track events. Results on preamp amplification and preamp linearity from the analysis of test-charge injection data of all six TPC sectors are presented. The minimal expected error on the measurement of signal charges in the TPC is discussed. Results are given on the application of the CDM Xtalk correction to test-charge events and krypton events.

1   Introduction

This memo is a sequel to two earlier memos on the TPC Xtalk correction [1, 2]. However, while the understanding of the electronics origin of the Xtalk problem is largely unchanged [3, 4], a novel concept for its correction is presented in this memo.

After explaining why a novel approach to the Xtalk problem was deemed necessary, the CDM (CERN-Dubna-Milano) correction algorithm is introduced.

Results of its application to various data sets with increasing complexity are presented.

2   A brief reminder on Xtalk

Shortly after the TPC Xtalk problem was realized in the spring of 2002, it could be satisfactorily explained by unwanted capacitive couplings from preamp outputs to preamp inputs [3]. The origin of the capacitive coupling is partly inside the multi-layer motherboard, partly within the ASIC chip which houses four preamps each.

The Xtalk problem was too large to be ignored, and it was clear from the beginning that a suitable algorithm had to be developed to correct for Xtalk.

We classify Xtalk in three classes: **unidirectional, self and bidirectional Xtalk.** Except for self Xtalk which involves one pad only, we distinguish between a **'leader' pad** (which is the intrinsic signal source) and its **'satellite' pad** (which is the recipient through capacitive coupling).

The three Xtalk classes are shown schematically in Fig. 2. We note that in the unidirectional and bidirectional cases, we deal with **pulse differentiation**, however in the case of self Xtalk we deal effectively with an operational amplifier, and therefore with **pulse integration.**

In practice, the three Xtalk classes tend to show up not isolated from each other but co-existing: any two, or all three of them (Fig. 2).

Besides the appearance of both differentiation and integration, and the co-existence of several Xtalk classes, a third important aspect for Xtalk correction algorithms is that the preamp inverts polarity, however the TPC ADC digitizes signals of negative polarity only.

Starting from the intrinsically positive input signal: the output signal is negative. The '1st-generation' unidirectional Xtalk signal is positive, with a negative undershoot from differentiation. The '2nd generation' unidirectional Xtalk is again negative, with a positive overshoot and a subsequent negative undershoot from differentiation. Since only negative signals are recorded, the direct signal and the unidirectional '2nd-generation' Xtalk signal look similar, whereas the unidirectional '1st-generation' Xtalk signal looks quite different.

This complex situation renders the understanding of the pulse shape of the leader pad a non-trivial problem, because of the possible superposition of self Xtalk and bidirectional Xtalk with one or several satellite pads, each with its own amplitude. To illustrate this problem, we give in Fig. 2 two pulse shapes in leader pads as observed with test-charge injection, a
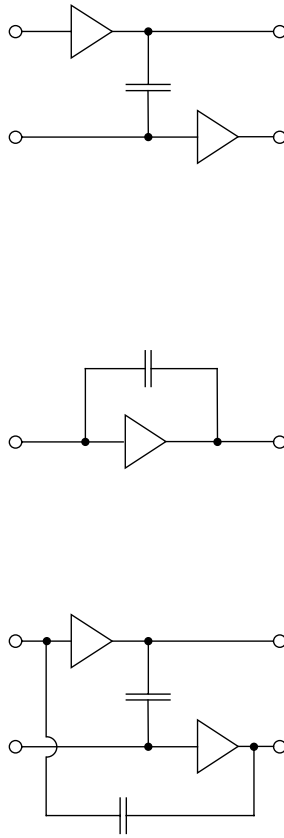
Figure 1: The three Xtalk classes: unidirectional (top), self (middle) and bidirectional (bottom); except for self Xtalk, the upper preamp refers to the leader pad, the lower preamp to the satellite pad.

'normal' and an 'abnormal' one. The normal case is, unfortunately, the exception rather than the rule.

We also show in Fig. 2 four pulse shapes in satellite pads, of which only the top left one is the one expected from differentiation of a normal leader pad pulse. Again, the normal case is the exception rather than the rule.

We concluded from the inspection of test-charge data that de-convoluting the pulseshapes of the satellite pads of a given leader pad is next to impossible: by contrast to the situation in a leader pad, in a satellite pad arises the additional complication that the pad receives input from other pads at 1st, 2nd, 3rd, etc. Xtalk generation levels, each with its own amplitude and its generation-specific pulse shape, possibly modified by self Xtalk.

Finally, it should be kept in mind that self Xtalk cannot, by principle, be corrected and must be considered an intrinsic feature of a preamp.
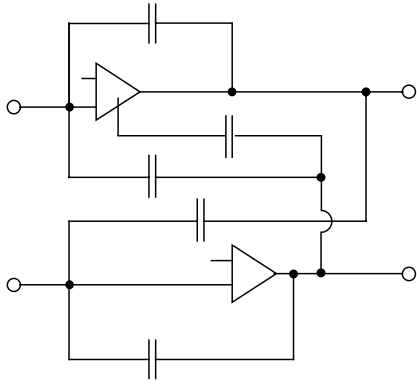
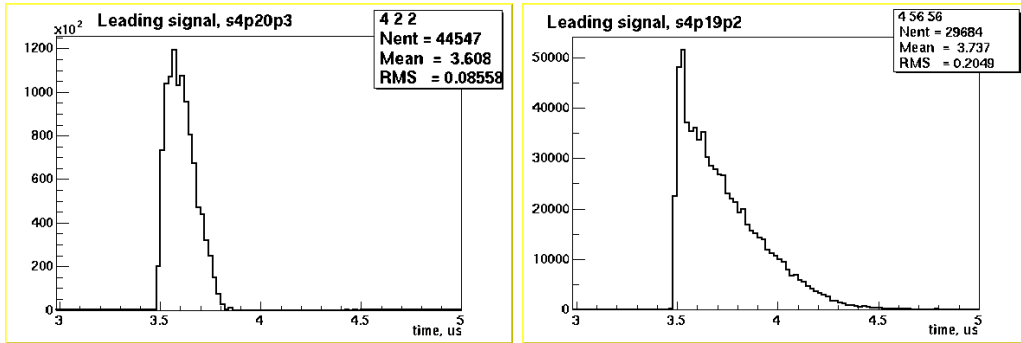Figure 2: A situation with co-existence of several Xtalk classes.

Figure 3: Shapes of leader pad pulses as recorded by the TPC ADC; normal case (left) and abnormal case (right).

3   Considerations on Xtalk correction algorithms

It was U. Gastaldi who presented a first idea to correct for the observed Xtalk. We call his proposal the 'Matrix Approach' [5]. It has recently been followed up by M. Apollonio, P. Chimenti, G. Catanesi and P. Temnikov [6].

In the Matrix Approach, the observed **time-integrated** charge in a given leader pad is described as a linear superposition of physics charges in the same pad and in other satellite pads, with individual amplitude coefficients. Thus, with 662 pads per TPC sector, the wanted physics charges can be obtained from the observed charges by the inversion of the 662×662 matrix of amplitude coefficients. This matrix is derived from test-charge injection data. Most of the amplitude coefficients are expected to be zero, and the inverted matrix needs to be established once only.

This approach has the appealing feature that automatically all Xtalk generations are taken into account.

Yet we discarded the Matrix approach for the following reason: **it permits the consideration of time-integrated charges only.** In reality, however, a given pad may receive an Xtalk contribution from the late signal in one pad, and from a concurrent early signal in another pad. Consideration of the time development of signals requires time-dependent am-
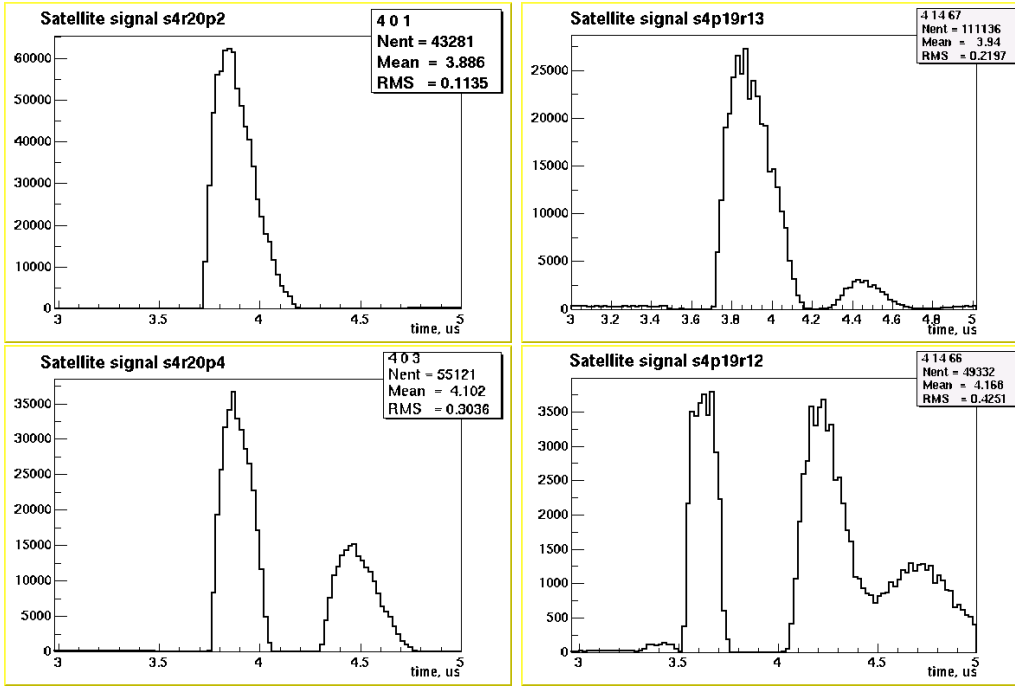
3

Figure 4: Shapes of satellite pad pulses as recorded by the TPC ADC; normal case (overshoot from 1st-generation unidirectional Xtalk; top left), abnormal cases (others).

plitude coefficients which render the Matrix Approach unmanageable already in case of two physics signals shifted in time with respect to each other, not to speak of more complicated cases in the busy TPC region around the target, where several tracks emerge close to each other.

We concluded that ignoring the time dependence of the Xtalk correction incurs a both unjustified and unnecessary loss of precision.

The second approach to Xtalk correction was a mathematical formulation of the differentiation of pulse shapes (the RC time constant involved is small enough that mathematical differentiation is justified). The approach starts from an arbitrary smooth pulse shape in the leader pad and derives from there by means of differentiation in Fourier space, and the introduction of coupling capacities for relative normalization between signals from leader and satellite pads, the pulse shapes of satellites with 1st- and 2nd-generation Xtalk signals. The procedure is decribed in G. Vidal Sitjes' PhD thesis [7], and in a recent note by G. Vidal Sitjes *et al.* [8].

Recently, it was proposed by M. Chizhov [9] to employ the Laplace transformation rather than a Fourier transformation. That is a change of mathematical procedure but not of the principle of deriving the pulse shape of satellite pads from the pulse shape of the associated leader pad.

The Fourier Transformation approach has the appealing feature that it takes automatically the time dependence of the pulses into account.

Yet we discarded the Fourier Transformation approach for three reasons.

4

- In order to derive the coupling capacities, the pulse shape of satellite pads must be deconvoluted into the unidirectional Xtalk contribution from the leader pad, and Xtalk contributions from other pads which each have generation-specific pulse shapes with individual amplitudes. We felt that the practical difficulties with disentangling all these effects were too large;

- Satellite pads may be individually affected by self Xtalk. Since the shape caused by self Xtalk is caused by integration and not by differentiation, self Xtalk in a satellite pad cannot be modelled by differentiation of the pulse shape of the leader pad;

- The Fourier Transformation approach suits well-behaved, smooth signals, for which the test-charge data are a good approximation. In real data, this is not the case: the TPC signal consists of δ-function like pulses spaced by 100 ns, with amplitudes which tend to be rather irregular functions of time – a situation where the Fourier Transformation approach will get into difficulties.

Facing this situation, we concluded that a new approach should be adopted which avoids what we felt were unnecessary shortcomings of the two earlier approaches. This resulted in the CERN-Dubna-Milano (CDM) approach to Xtalk correction. Our approach applies the Xtalk pattern, experimentally determined with test charges, in a straightforward way to data. The time dependence of the Xtalk correction is fully respected. The computational overhead is minimal.

4   Test-charge data reduction

With a view to an experimental determination of the Xtalk pattern, a δ-signal of charge Q was injected by a pulser into each of the 662 pads of each of the 6 TPC sectors [10]. **The test charge Q is conjectured to be the same for all pads** (the signal probe was designed to have by means of a spring well-defined ohmic contact with the pad).

This conjecture is likely to be correct, however beware that there is no unambiguous proof.

The 'Phase-lock technique' was employed: 2500 events were taken for each pad, each with a different but measured time delay. Thus a smooth output pulse shape could be constructed from the superposition of many events despite of the coarse 100 ns sampling of an individual event.

In addition to the signal of the leader pad into which the test charge was injected, the signals of all other 661 pads of the respective TPC sector were recorded.

The typical pulseheight of the time-integrated signal was 800 ADC counts, the typical height of a sampling pulseheight was 300 ADC counts (the maximum ADC count is 4095).

In addition to the injection of the charge Q, charges $Q/2$ and $Q/4$ were injected, with a view to assessing the linearity of the preamps.

This campaign produced ~ 0.8 TB of raw data.

In a first pass which took 360 hours of PC time, the individual events were reduced to histograms of 10 μs length, in bins of 20 ns, for each leader pad and each satellite pad; this resulted in $\sim$ 7 GB of data.

The program used for the data reduction was adapted from a program originally developed by one of us (A.K.) for the monitoring of the NDCs.

In a second pass, the results of a pattern recognition of the histogrammed signal shapes were stored in a ROOT tree; this resulted in $\sim$ 10 MB of data.

5 3 μs problem, 100 ns problem, pedestal problem

The inspection of the histograms confirmed an earlier observation [11] that in some events the timing signal of an overall delay of the TPC pulse train of $\sim 3\mu$s was missing, and that some pads were affected by an advance of the signal by 100 ns (which is the period of TPC pulse sampling).

Both effects are still under investigation. While the missing $\sim 3\mu$s timing signal poses no problem because of the good overall stability of the system, the cause of the 100 ns problem is still unclear. At this point in time, no correction recipe is known. However, its effect on the data is equivalent to a 5 mm shift of the pad signal in the upstream direction, and therefore not dramatic.

On assumption (which is not unambiguously proven) that the 100 ns problem is stable with time, all subsequent considerations, especially on Xtalk correction, remain valid, since the CDM algorithm has no *a priori* notion on the relative timing between the signal of leader and satellite pads.

Yet another problem apparent in the test-charge data is some uncertainty in the ADC pedestal substraction.

At every new run (in the test-charge data taking campaign, changing to a new pad meant starting a new run), first the pedestal of each ADC is determined from the average of a number of 'pedestal events'. During readout, this pedestal is subtracted from the data, but its value can be reconstructed from the offline analysis of pedestal events. There is no reason to suspect that something went wrong, however we note that the pedestal values in TPC sector 5 were systematically much higher than the pedestal values in the five other sectors during the test-charge data taking.

When determining the time-integrated pulseheight from the histograms, for each bin it must be decided whether to take its charge into account or not, because a non-zero threshold is mandatory in order to discriminate against digitization fluctuations and white noise. The adopted procedure was to accept the recorded charge inside a 100 ns bin in case its ADC count was above 10. However, the choice of the numerical value of this threshold is nontrivial, as it introduces a small systematic loss of charge, and small fluctuations which we estimate at the $\sim$ 2% level. More work is needed before settling on a final, optimum and coherent choice.

6 Classification of pad channels

The test-charge data permit the classification of TPC pads into four groups:

- **Missing pad:** a pad is called 'missing' if it is not found in the Q sample;

- **dead pad:** a pad is called 'dead' if its integrated charge is less than 100 ADC counts;

- **Noisy pad:** a pad is called 'noisy' if its integrated charge is above 100 ADC counts and has high ADC counts throughout;

- **Good pad:** a pad is called 'good' it it does not belong to any of the three other categories.

Table 6 gives the number of pads in each category, for each of the six TPC sectors.

Table 1: Numbers of pads in different categories, for each TPC sector.

Sector	TPC pads			Good	Good(%)
	Missing	Dead	Noisy	Good	Good(%)
1	1	9	4	648	97
2	0	69	15	578	87
3	1	13	8	640	97
4	1	10	5	646	97
5	5	40	34	583	88
6	5	5	0	652	98
1-6	13	146	66	3747	94

Figure 5 shows the location of dead pads in the TPC sectors.

We would like to stress that noisy pads require careful attention, because when determining an Xtalk pattern, they show up as fake satellite pads to **every** leader pad, and therefore would give rise to large Xtalk corrections which are entirely fake.

7 Preamp gain

On assumption that the **same** test-charge is injected into each pad, the integrated output charge measured in ADC counts determines directly the preamp gain, apart from an (irrelevant) overall normalization factor.

It was argued before [2] that one should consider 'effective' gains, defined as gains inclusive of Xtalk. This definition leads to a contradiction: after correction for Xtalk, when the gain equalization is to be applied, it should refer to Xtalk-corrected charges; but the 'effective' gain was determined from Xtalk-affected charges!
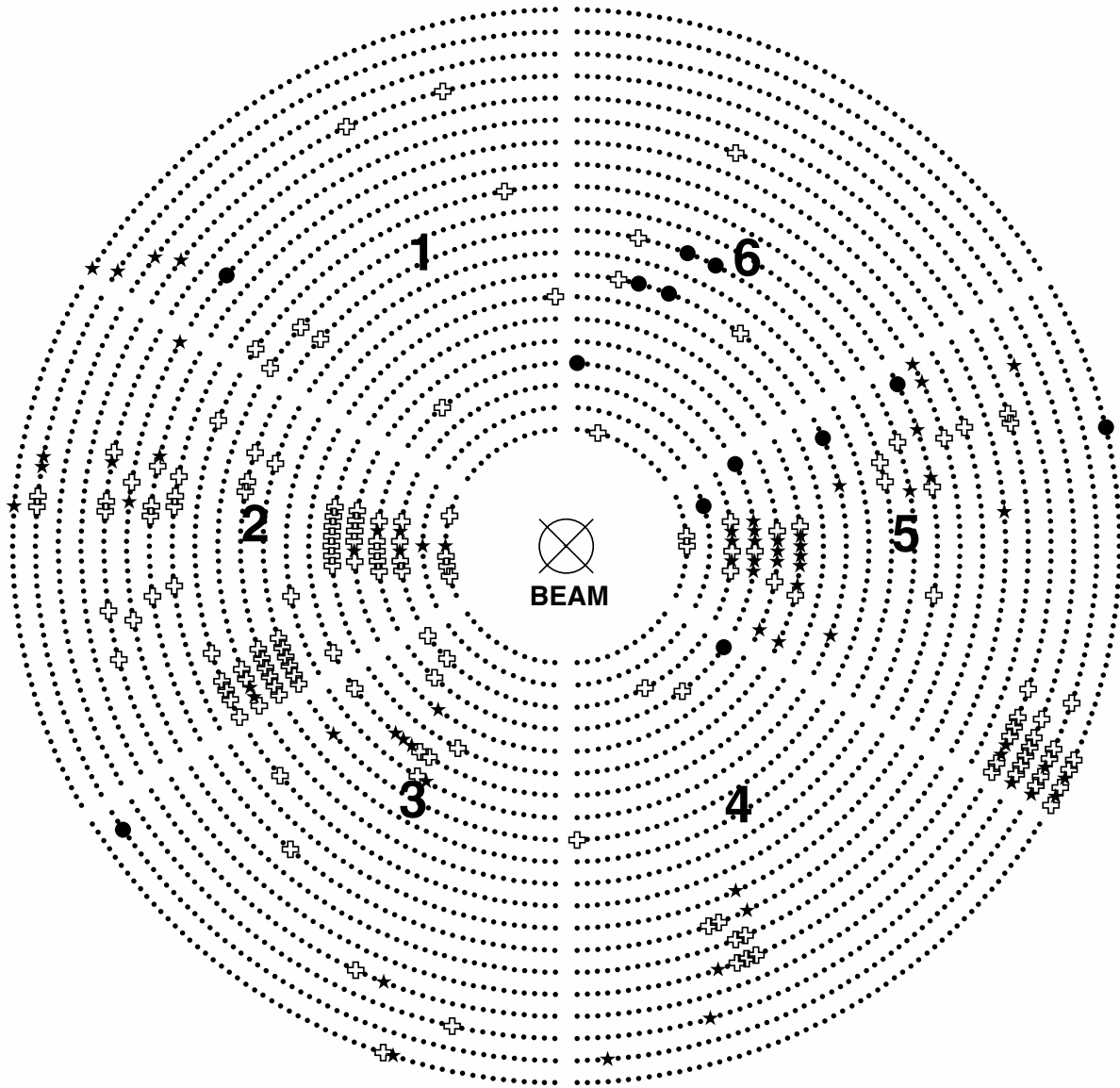
Figure 5: Location of missing pads (full dots), dead pads (open crosses) and noisy pads (stars) in the TPC sectors, as determined with test-charge injection.

Therefore, the gain equalization is to be made on the basis of charges already corrected for Xtalk.

We chose to determine the Xtalk-corrected gains from the integrated charge of each leader pad, within a tight time cut around the first signal maximum, so as to minimize the influence of Xtalk which is – except for self Xtalk – time-delayed. As said already above, the effect of self Xtalk cannot be unfolded by principle, and must be treated as an intrinsic property of the pertinent preamp.

The resulting preamp gains are shown in Fig. 6 for TPC sectors 1–3, and in Fig. 7 for TPC sectors 4–6. We recall that the abolute normalization is arbitrary. Most of the pads are well-behaved, however there is an unpleasant tail toward small gain.

The preamp gains cluster around an average value of ~ 800 ADC counts, except in sector 5 cluster where they cluster around 600 ADC counts. At higher than average gain, secondary clusters are visible which are traced back to pulses with larger widths, originating from self Xtalk that makes the preamp appear to have higher gain. Thus, the relative importance of self Xtalk can be assessed.

8   Preamp non-linearity

The output stage of the preamp is an emitter follower, with a small current through the emitter such that the emitter diode is 'just' open. The current is regulated by the voltage level at the basis, which undergoes small variations as it is not stabilized against temperature changes. Therefore, because of either a small mis-adjustment of this voltage level, or because of a change of ambient temperature, the emitter diode can go from the nominal 'open' state to a state where it starts to close.

Whereas in the normal state the integral linearity of the preamp is expected, and verified in laboratory measurements to be good within a few percent, in some cases a non-linearity of the preamp will show up. Unfortunately, stability with time cannot be expected for this effect.

To get an idea of the extent of the preamp non-linearity, at least during the winter months of January and February 2003, test-charges with value $Q/2$ and $Q/4$ were injected in addition to the charge Q.

Figure 8 shows for all six sectors the ratio of the responses of $Q/2$ and Q injection, Fig. 9 shows the same for the ratio of responses of $Q/4$ and Q injection. While most of the pads are well-behaved, several percent of them show a large deviation from linearity.

Sector 5 sticks out from the sectors by worse fluctuations.

9   The CERN-Dubna-Milano algorithm

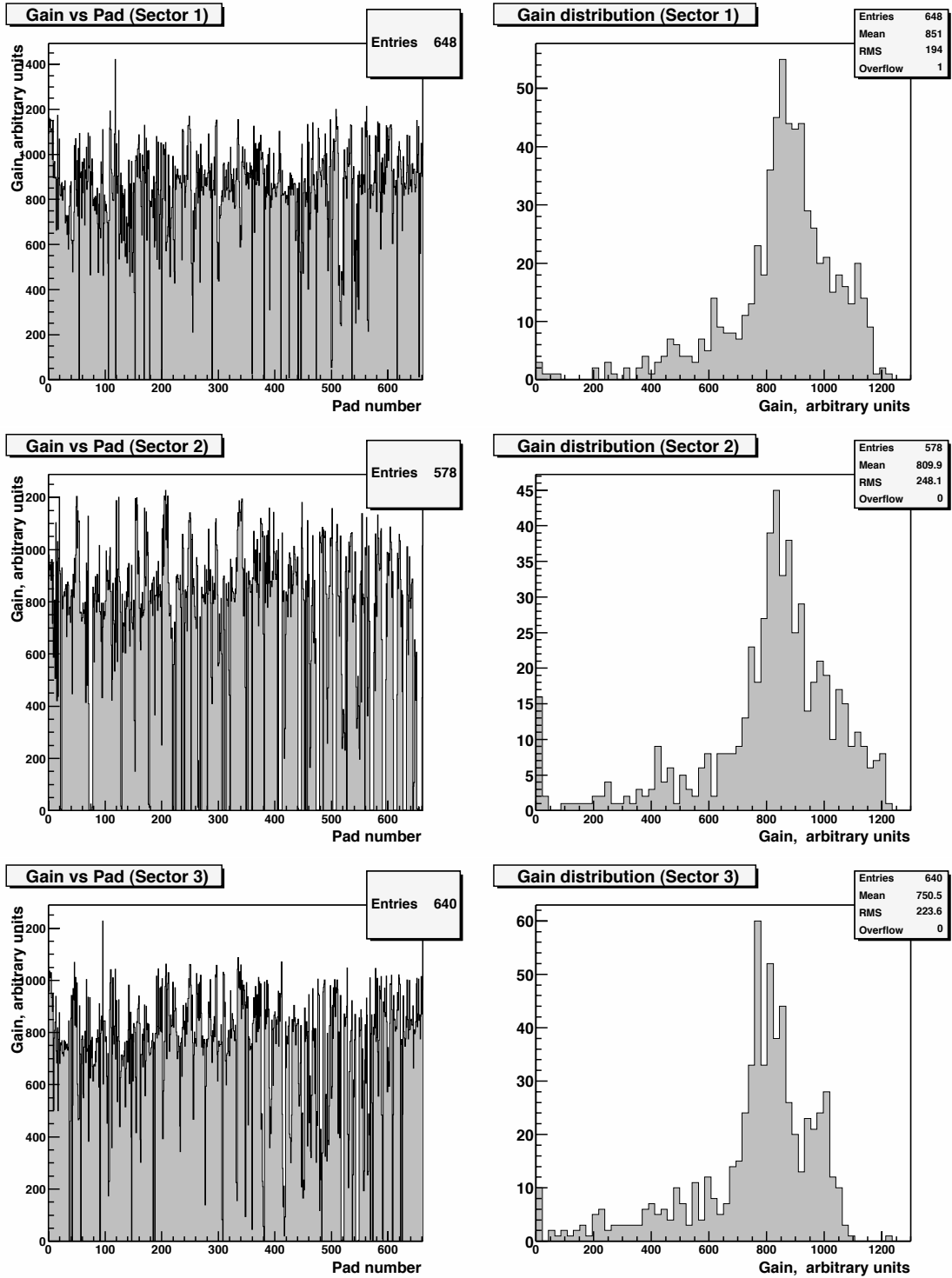The CDM Xtalk correction algorithm comprises two steps which are described in turn.

Figure 6: Preamp gains versus pad number for TPC Sectors 1–3; differential distributions (left) and projections (right).
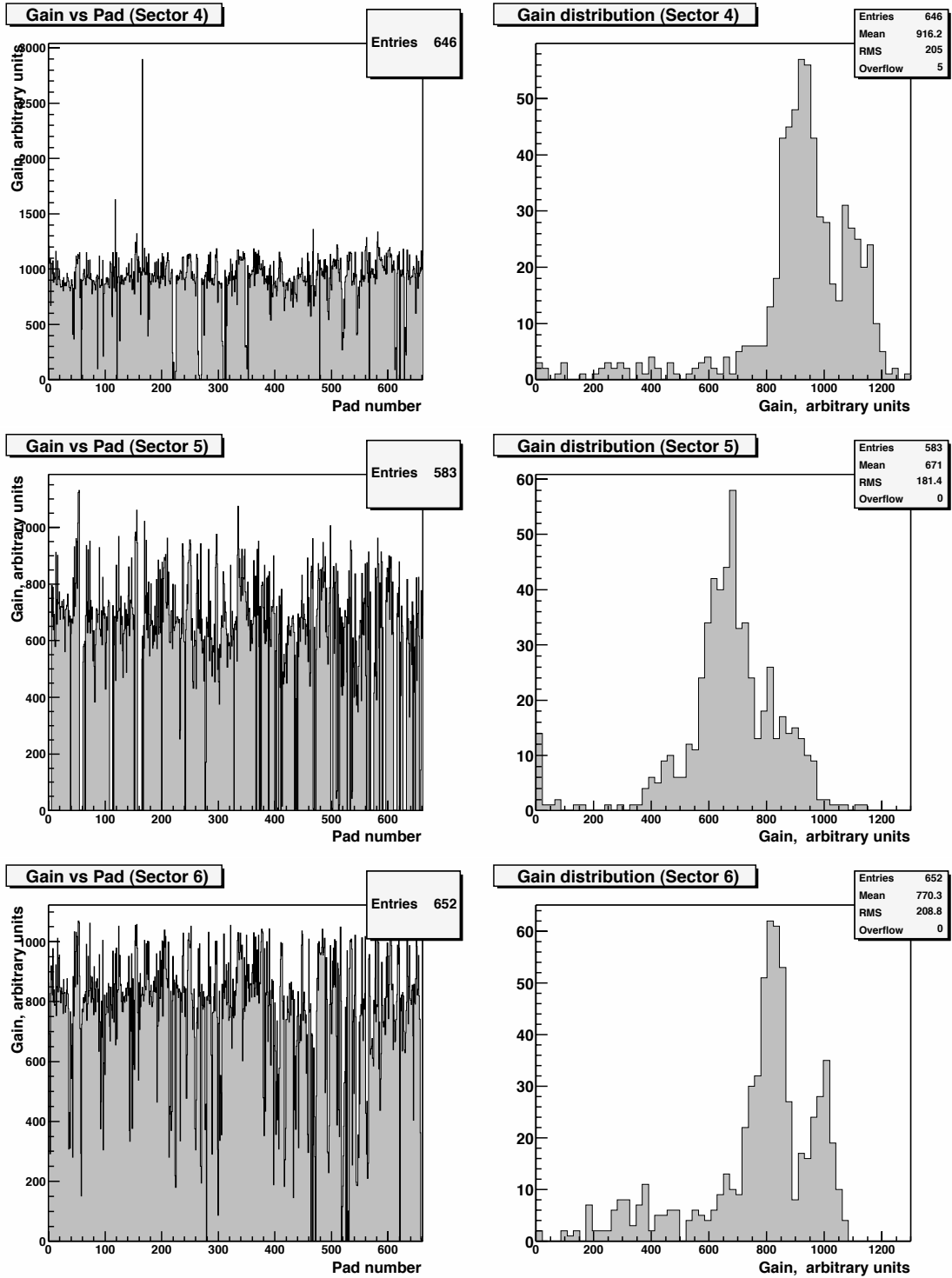
Figure 7: Preamp gains versus pad number for TPC Sectors 4–6; differential distributions (left) and projections (right).
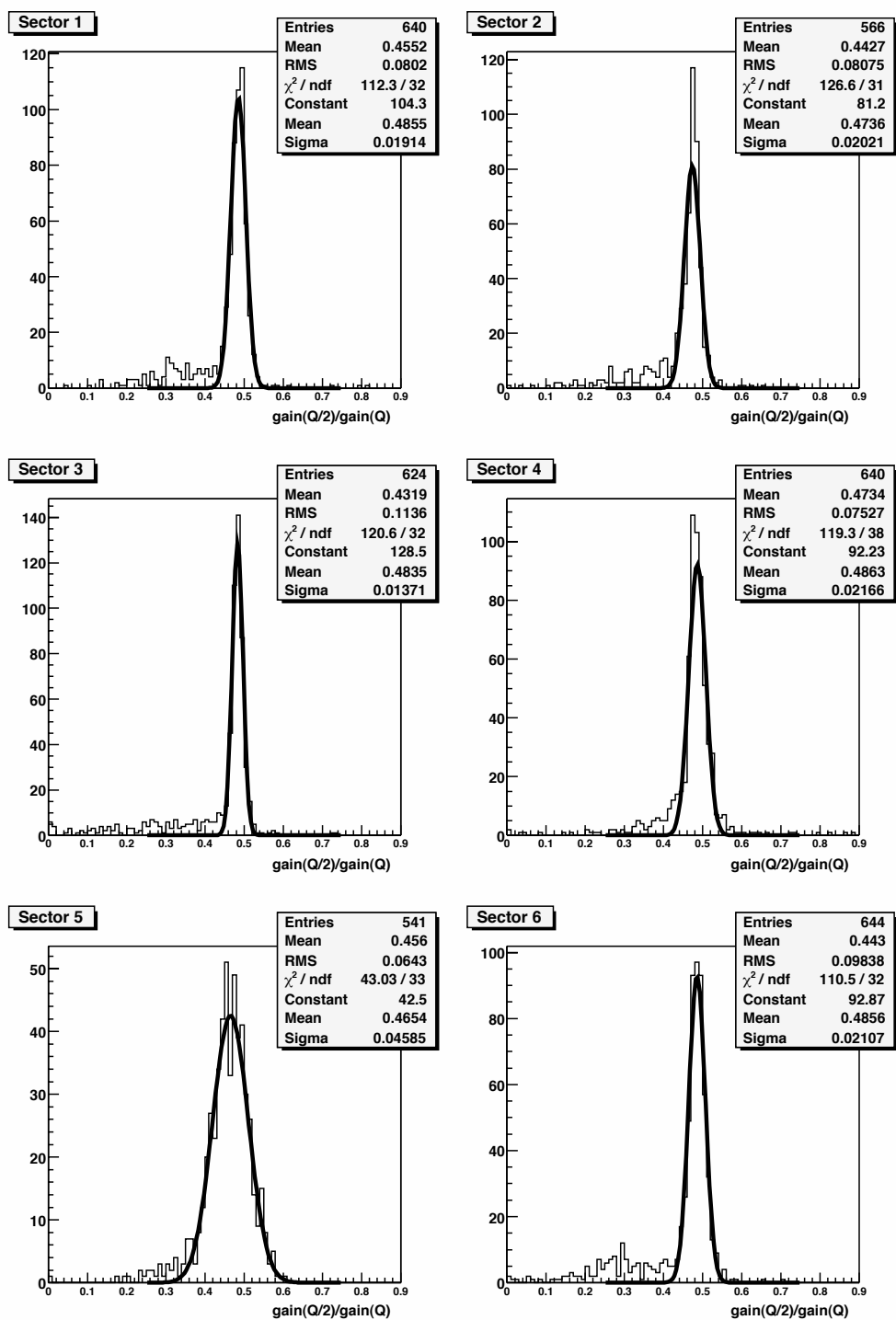
Sector 1

Entries	640
Mean	0.4552
RMS	0.0802
χ^2 / ndf	112.3 / 32
Constant	104.3
Mean	0.4855
Sigma	0.01914

gain(Q/2)/gain(Q)

Sector 2

Entries	566
Mean	0.4427
RMS	0.08075
χ^2 / ndf	126.6 / 31
Constant	81.2
Mean	0.4736
Sigma	0.02021

gain(Q/2)/gain(Q)

Sector 3

Entries	624
Mean	0.4319
RMS	0.1136
χ^2 / ndf	120.6 / 32
Constant	128.5
Mean	0.4835
Sigma	0.01371

gain(Q/2)/gain(Q)

Sector 4

Entries	640
Mean	0.4734
RMS	0.07527
χ^2 / ndf	119.3 / 38
Constant	92.23
Mean	0.4863
Sigma	0.02166

gain(Q/2)/gain(Q)

Sector 5

Entries	541
Mean	0.456
RMS	0.0643
χ^2 / ndf	43.03 / 33
Constant	42.5
Mean	0.4654
Sigma	0.04585

gain(Q/2)/gain(Q)

Sector 6

Entries	644
Mean	0.443
RMS	0.09838
χ^2 / ndf	110.5 / 32
Constant	92.87
Mean	0.4856
Sigma	0.02107

gain(Q/2)/gain(Q)

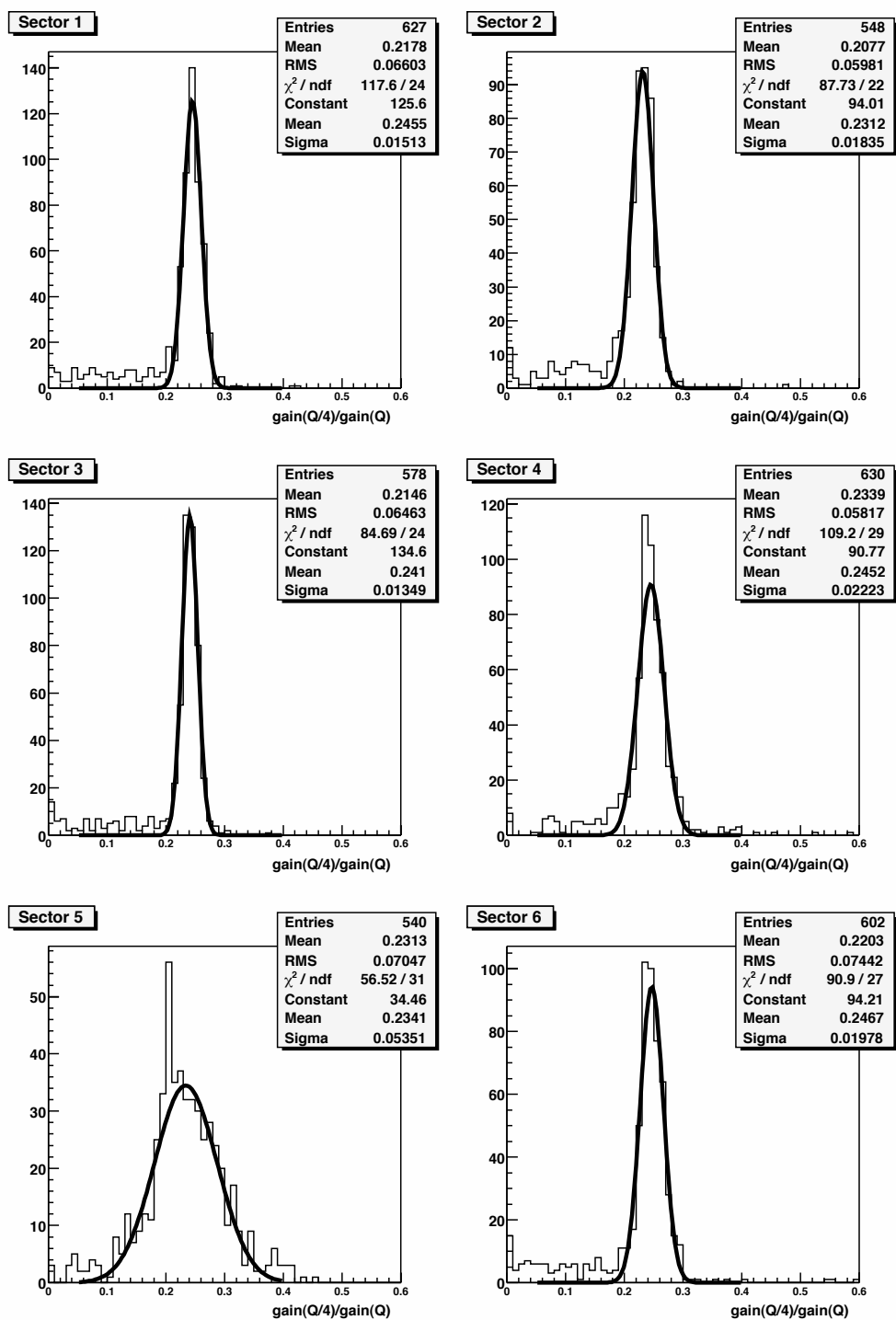Figure 8: Ratio of preamp responses to $Q/2$ and Q injection, for all six TPC Sectors.

Figure 9: Ratio of preamp responses to $Q/4$ and Q injection, for all six TPC Sectors.

An important consideration is pad equalization: the CDM Xtalk correction algorithm works at the ADC count level. There is no attempt of pad equalization throughout the whole procedure.

9.1 Step 1: Construction of Xtalk maps

The test-charge histograms (which are binned in 20 ns intervals) of each leader pad are re-binned in 100 ns intervals by adding the charges of five adjacent bins. The borders of the 100 ns bins are defined such that the earliest border is located 140 ns earlier than the early 20 ns bin border which contains the peak of the pulse.

A 2-dimensional map of L_{ij} is stored for each TPC Sector, where i denotes the pad number (i = 1...662) and j the time bin, up to a maximum length of 2 μs. For a L_{ij} to be non-zero, the ADC count must be larger than 10.

The L_{ij} are then renormalized, such that the value of the first bin is unity.

In the same way, with the same binning inside the same 2μs interval, the charge distributions of all satellite pads are stored in 3-dimensional maps of C_{ijk}, where the third index k denotes the satellite pad number. Again, for a C_{ijk} to be non-zero, the ADC count must be larger than 10.

The C_{ijk} are renormalized by the same factor as the L_{ij}. In this way, the measured ratio of charges between the leader pad and the satellite pad is preserved.

We stress the following features:

- the maps define at the same time which satellite pads belong to which leader pad;

- **any** observed pulse shape is accepted; there is no prejudice regarding the generation level of Xtalk; there is no prejudice regarding the presence or absence of self Xtalk; there is no prejudice regarding the presence or absence of the 100 ns problem;

- the time dependence of the pulses as well as the time relation between leader pad and satellite pad pulses is fully respected.

9.2 Step2: Application of Xtalk maps

First, we determine the overall characteristics of the event in terms of 'hits'. Hits are defined, within a pad, as trains of pulses above a threshold. In real data, hits typically comprise several pulses spaced by 100 ns, with a rather erratic time dependence. A smooth time dependence is the exception rather than the rule.

The hits are then time-ordered. The Xtalk correction proceeds with a loop over hits according to their time order.

In the loop over hits, suppose to have arrived at a given hit in a given pad. In the following, this pad is referred to as leader pad. Its charge is by definition non-zero and we aim at correcting other pads for Xtalk produced by the charge in the leader pad.

We investigate by inspection of the Xtalk maps, whether the leader pad is affected itself by Xtalk from another pad, and which if any satellite pads are affected by the leader pad. We distinguish three mutually exclusive cases.

- **Case a:** The leader pad is not affected by Xtalk from another pad. In this case we know that the charge observed in the leader pad is a pure physics charge, and the Xtalk pattern as observed with test-charges directly applies, with no regard of the Xtalk generation.

The application of the Xtalk correction now faces the hurdle that what is measured (and available as the maps of L_{ij} and C_{ijk}) is derived, and refers to, a **smooth** time dependence of pulses spanning several 100 ns bins. On the other hand, the practical application to real data is to a pulse within a pulse train with 100 ns spacing with – in general – irregular time dependence. The problem is how to associate a single pulse within a pulse train with the Xtalk maps.

This problem has been pragmatically solved in the following way [12]. **The irregular pulse train of the data is considered as superposition of as many L_{ij} signals as the hit has 100 ns bins, with varying amplitudes and positive or negative signs as suitable.**

We start with the first time bin of the data. The L_{ij} (we recall that they are normalized such that the first time bin is unity) are normalized to the data pulseheight in this bin, and subtracted from the data bin by bin. The first bin will by construction have zero content after the subtraction, whereas the subsequent time bins will have reduced and possibly even negative charge. Negative contents are retained as such.

The same normalization factor is applied to the C_{ijk} and for each satellite pad the predicted Xtalk charge from the first time bin of the data is calculated.

We repeat the same procedure with the second time bin, with the normalization determined by the remaining charge in the second time bin. If this charge happens to be negative, the same procedure is carried out with a negative sign.

This way, we work through all time bins of the hit. Finally, the Xtalk predictions from each time bin are added up. The resulting Xtalk predictions are for the time being retained separately from the observed charges.

The procedure is entirely model-independent and simply emulates the flow of Xtalk charges from the leader pad to the satellite pads. It preserves by construction the relative amplitudes and time dependences. There is no attempt to fit the pulse shapes in the framework of a model.

- **Case b:** This case applies when the leader pad is found in the maps as the satellite of another pad, but in the particular hit, this other pad has zero charge and therefore the leader pad is not affected by Xtalk from this pad. The situation becomes congruent to Case a. Accordingly, the same procedure as in Case a is applied.

- **Case c:** This case applies when the leader pad is found in the maps as the satellite of another pad – which we call in the following parent pad – which has a non-zero charge (there may be several parent pads: in this case, the following procedure is repeated for each

15

parent pad). There are two possibilities: (i) there exists already a predicted Xtalk charge for the parent pad resulting from an earlier step in the loop over hits, or (ii) there is no such prediction. In the former case, we subtract bin by bin the predicted Xtalk charge from the observed charge and consider the remainder as pure physics charge. In the latter case, we make consciously a hopefully only small error and treat the observed charge as pure physics charge, although it may have an Xtalk contribution from yet another pad.

In either case, we apply the Xtalk maps to calculate in turn the following:
– first, the Xtalk charge in the leader pad which is induced by the charge in the parent pad;
– second, the Xtalk charge in all satellite pads of the leader pad which are induced by the charge in the parent pad;
– third, after subtracting the predicted Xtalk charge in the leader pad and thus obtaining its pure physics charge, the Xtalk charges in the satellite pads induced by the pure physics charge of the leader pad.

This rather involved procedure is implemented because of the polarity inversion of the preamp, which calls for the consideration of Xtalk across at least two generations. Notice that the Xtalk maps determined from the test charges define in the first generation only the Xtalk charges resulting from physics charges, not from Xtalk charges. Xtalk charges induced in the next generation by Xtalk charges are not described by the Xtalk correction maps!

In all three Cases a, b and c we calculate only Xtalk charges for the **satellites** of the leader pad. If in Case c an Xtalk charge in the leader pad is calculated, it is deleted again when leaving the leader pad, in order to avoid multiple corrections. (The correction will be calculated at a later time, when the loop over hits will make the former parent pad to the leader pad, and the former leader pad to a satellite pad).

At the end of the loop over hits, in a second loop, the calculated Xtalk charge profiles are subtracted, bin by bin, from the observed charge profiles. After the subtraction, only pure physics charges remain.

At this point in time, after the Xtalk correction procedure is completed, a pad equalization can be applied which is a precondition for observing physics effects like a krypton energy spectrum.

Perhaps interesting from a practical point of view: because the CDM algorithm involves very simple algebraic operations only, it consumes very little computing time.

10   Results of CDM algorithm: test-charge data

Any Xtalk correction algorithm must pass a first test: to correct test-charge injection data for Xtalk. Passing this test is necessary but not sufficient, since the configuration of test-charge events is the easiest possible: one single pad is excited only, and only one 'event' in the whole TPC volume is created.

Figure 10 shows the observed Xtalk charges in satellite pads against the calculated Xtalk

charges. The concentration at the diagonal shows that in the grand majority of cases, the Xtalk charge is calculated correctly. The band below the diagonal arises from one noisy channel only which had not yet been eliminated when creating the plot, with a view to underlining the necessity to treat noisy channels with great care.

Figure 10 shows the ratio of the Xtalk charge to the average charge in the leader pad, per satellite pad, before and after the Xtalk correction. After the Xtalk correction, one expects this ratio to average at zero, with as small a fluctuation as possible. The fluctuation of this ratio is important for its impact on the precision of the azimuthal coordinate measurement in the TPC (note that the fluctuation is larger because, for technical reasons, the normalization is to the average charge and not to the individual charge of the leader pad).

11   Expected precision of charge measurement

The precision of a charge measured in the TPC is affected by four factors:

- the precision with which the ADC pedestal was subtracted at readout time, and the choice of the threshold ADC count. We guess that this causes fluctuations of charge measurement at the 3% level;

- the sampling of the pulse every 100 ns; originally, a charge integration in every 100 ns bin was planned which would have measured correctly the integral charge; however, due to practical constraints, a system had to be adopted which measured every 100 ns not the integrated charge but the **pulse height**; this introduces a sampling fluctuation which is the worse the shorter the pulse. Fig. 12 shows from test charge data the fluctuation of the charge of individual events with random time sampling, compared to the average charge. One deduces a $\sim 6\%$ resolution from this effect.

- the equalization of pad gains; this is best determined with krypton data and has a fluctuation of order 5% from statistics and systematic limitations;

- the Xtalk correction; from Fig. 10 we estimate that the Xtalk-corrected charges have a fluctuation of $\sim 5\%$ from inadequacies of the Xtalk correction.

Quadratically added, this gives a fluctuation of the charge measurement in the TPC of about 10%, which is irreducible.

For the krypton spectrum, an intrinsic physics resolution of the 41.3 keV peak of about 5% is to be added. Therefore, the best possible energy resolution of the 41.3 keV krypton peak is $\sigma \simeq 11\%$.

This fluctuation of the charge measurement in the TPC also transforms into a fluctuation of the azimuthal coordinate of the TPC. The $r\phi$ resolution from this effect is about 200 μm.

The dE/dx resolution of the TPC is expected to be seriously compromised by the expected charge measurement fluctuations.

12 Results of CDM algorithm: krypton data

After the internal consistency test provided by the application to test-charge data, the CDM Xtalk correction algorithm was applied to ^{83m}Kr data.

Periodically, data had been taken with radioactive krypton mixed into the TPC gas, with a view to equalizing and calibrating the response of each pad readout channel. Krypton decays produce charge deposits which are typically confined within a centimetre within the TPC gas volume. The ionization charge produced in a single decay event is spread over a few pads. A dedicated cluster-finding algorithm needs to be applied, and a pad equalization needs to be performed in order to observe the energy peaks of the krypton spectrum.

The typical pulseheight of the time-integrated krypton signal was less than 4000 ADC counts, the typical height of a sampling pulseheight was less than 1000 ADC counts.

The pad equalization constants are obtained as follows:

1. for each reconstructed cluster, the pad receiving the maximum amount of charge is identified as the 'leader' pad;

2. for each pad a histogram is created and filled with the charge collected on that pad when, and only when, it is the leader pad in a cluster;

3. all histograms are equalized in terms of mean (or median) value by means of a multiplicative factor; the inverse of this factor corresponds to the equalization constant for the respective pad.

The procedure is iterated several times until the equalization constants become stable.

Xtalk affects krypton data in two ways:

1. the pad multiplicity of krypton clusters is increased due to the appearance of satellite pads;

2. the krypton spectrum is distorted towards higher energy values, and the energy resolution is deteriorated.

The effect of the CDM algorithm on the krypton data collected in 2002 is shown in Figs. 12 and 12, which give the observed pad multiplicity and energy spectrum of reconstructed krypton clusters before and after applying the CDM algorithm, respectively.

The plots show that:

- the average multiplicity of pads associated to clusters is reduced by 20% when the CDM algorithm is applied;

- the krypton energy peaks are shifted towards lower values;

- the krypton spectrum shows an evident improvement, as the long tail at the right side of the plot is significantly reduced.

This permits the conclusion that the CDM Xtalk correction algorithm is successful.

On the other hand, we observe a slight deterioration of the 'core' resolution, i.e. in the region close to the peaks, as witnessed by the fact that the ~ 9 and ~ 12 keV peaks appear less separated after applying the CDM algorithm. This effect is currently under investigation. Unless imperfections are found in the algorithm implementation or in the krypton cluster-finding (which is indeed affected by the correction), the observed resolution might indicate the limits of the Xtalk recovery procedure.

The correlation between the equalization constants obtained with and without correction (Fig. 12) provides an estimate of the fluctuation introduced by the Xtalk correction in the equalization procedure ($\sigma \sim 5\%$).

Unexpectedly, the equalization constants obtained from the krypton analysis appear uncorrelated with those derived from the analysis of the test-charge data described above (Fig. 12). Currently, we have no understanding of this intriguing feature of the data. Investigations to elucidate the problem are under way.

13 Summary

A rather complete first analysis of the TPC test-charge data is presented which permits a classification of pads into quality classes, the determination of preamp gains and preamp non-linearities. Further, Xtalk correction maps were derived and applied to test-charge data themselves, and to krypton data. It is not yet understood why preamp gains from test-charge data appear uncorrelated with preamp gains from krypton data. Yet, applying the Xtalk correction according to the CERN-Dubna-Milano algorithm and using krypton equalization constants, the prominent tail of the krypton spectrum to high energy largely disappears.

References

[1] Implementation of the TPC crosstalk correction, revised edition of 11th September, 2002, by M. Chizhov *et al.*, *http://cern.ch/dydak/crosstalk.ps*

[2] The TPC Xtalk correction, by A. De Min and F. Dydak, *http://cern.ch/dydak/-crosstalk2.ps*

[3] We thank J.C. Legrand for his efforts to understand at grassroots level the origin of the TPC Xtalk, and his untiring readiness to discuss his findings with pedestrians.

[4] G. Vidal Sitjes, presentations in the September and December 2002 Collaboration Meetings.

[5] To our knowledge, the earliest written record of the Matrix Approach is in the Minutes of the HARP Group Meeting held on 2 April 2002, in an enclosed record of a dedicated meeting on Xtalk, held at CERN on 3 April 2002.

[6] M. Apollonio *et al.*, Status of X-Talk Correction, *http://gabri.home.cern.ch/gabri/- HARP/Reconstruction/27-may-2003/Xtalk.html*

[7] G. Vidal Sitjes, PhD Thesis, University of Valencia, 2002.

[8] G. Vidal Sitjes *et al.*, Status of TPC analog electronics cross-talk measurement, */afs/- cern.ch/user/b/bieluh/public/StatusOfXTMeasurement.ps.gz*

[9] M. Chizhov, Analytical treatment of the cross-talk, *http://evalu29.ific.uv.es/- harp_analysis/xtalk.htm*

[10] We thank V. Serdiouk who did during January and February 2003 the lion's share of this painstaking work, with impressive dedication and perseverance.

[11] We thank J. Burguet Castell for having pointed out this problem of the readout of TPC test-charge data.

[12] The idea was first proposed and put into practice by A. Guskov and A. Zhemchugov.
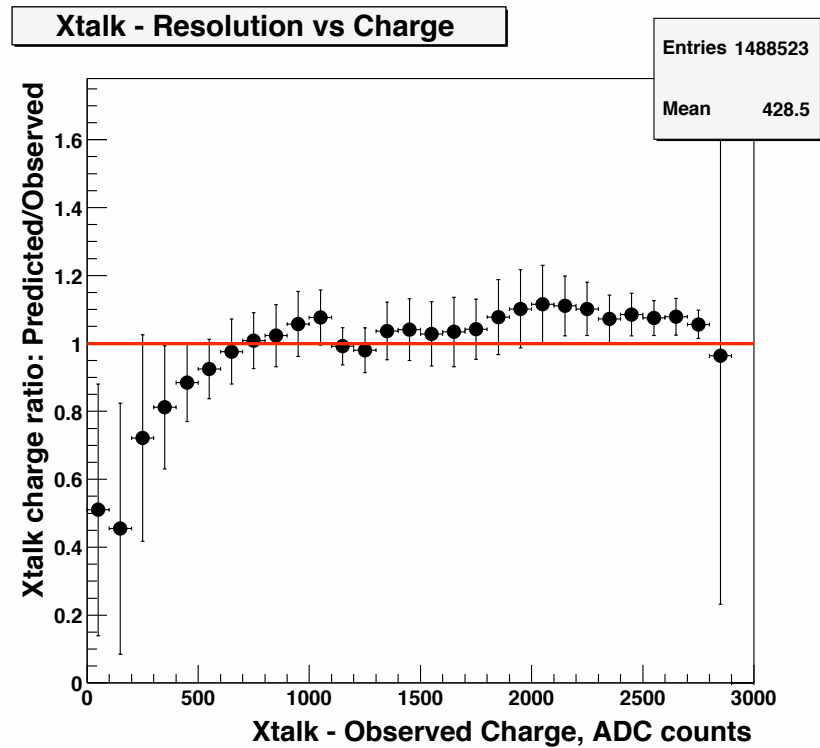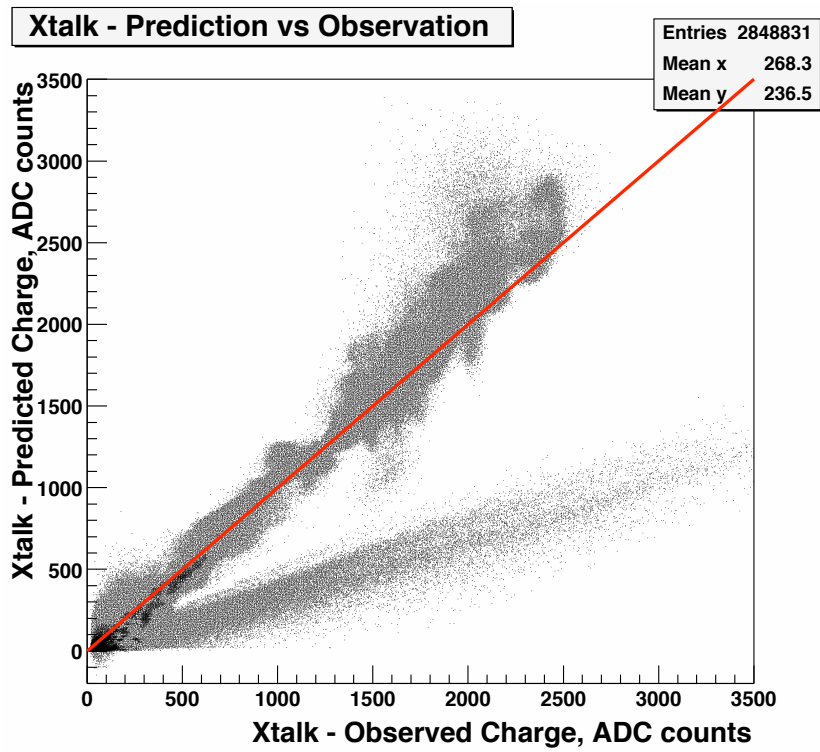
Figure 10: Calculated Xtalk charge versus observed Xtalk charge; the band below the diagonal is due to one noisy channel (top); ratio of the calculated to observed Xtalk, with noisy channel removed (bottom).
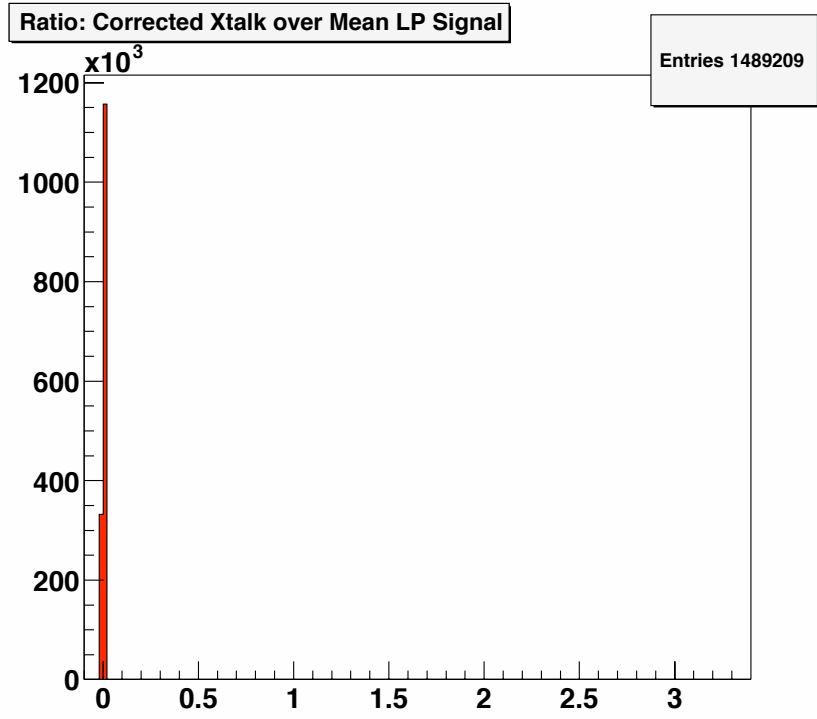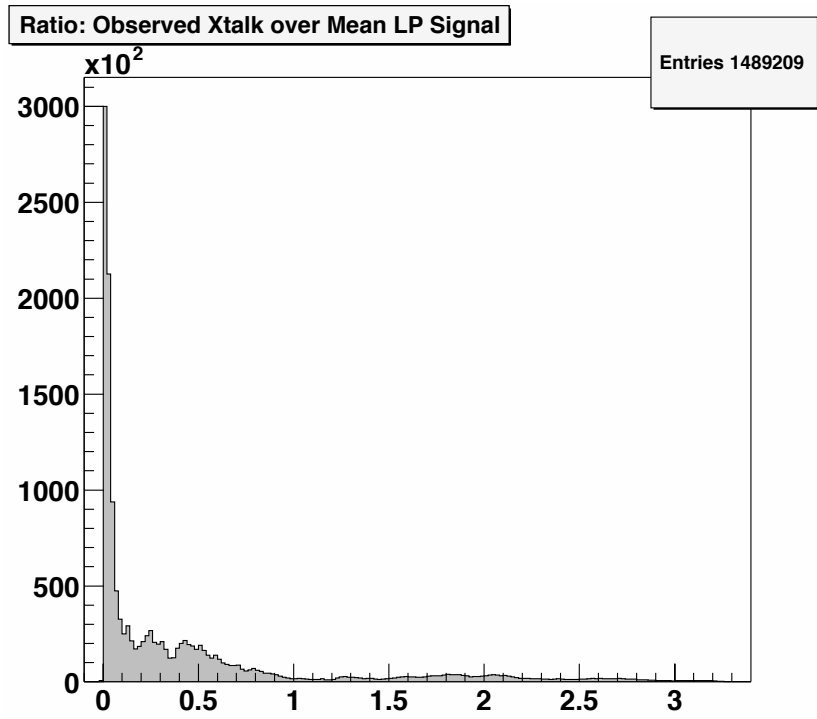
Figure 11: Ratio of the calculated Xtalk charge per satellite and the average charge of the leading pad, before (top) and after (bottom) Xtalk correction.
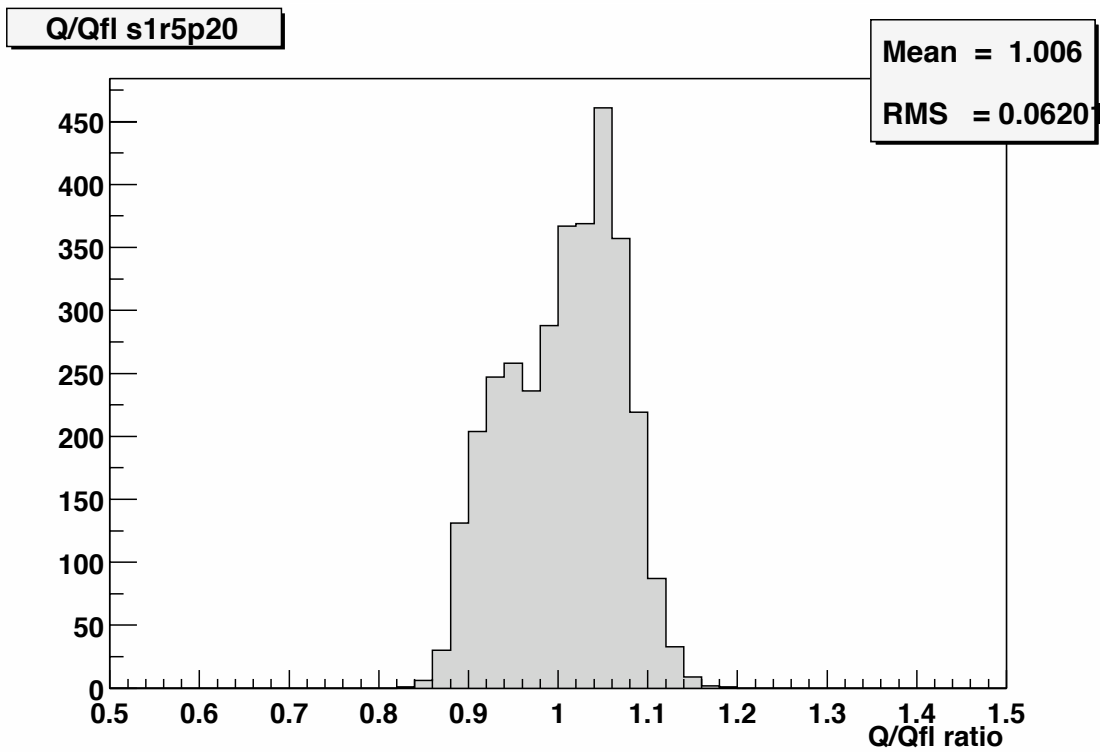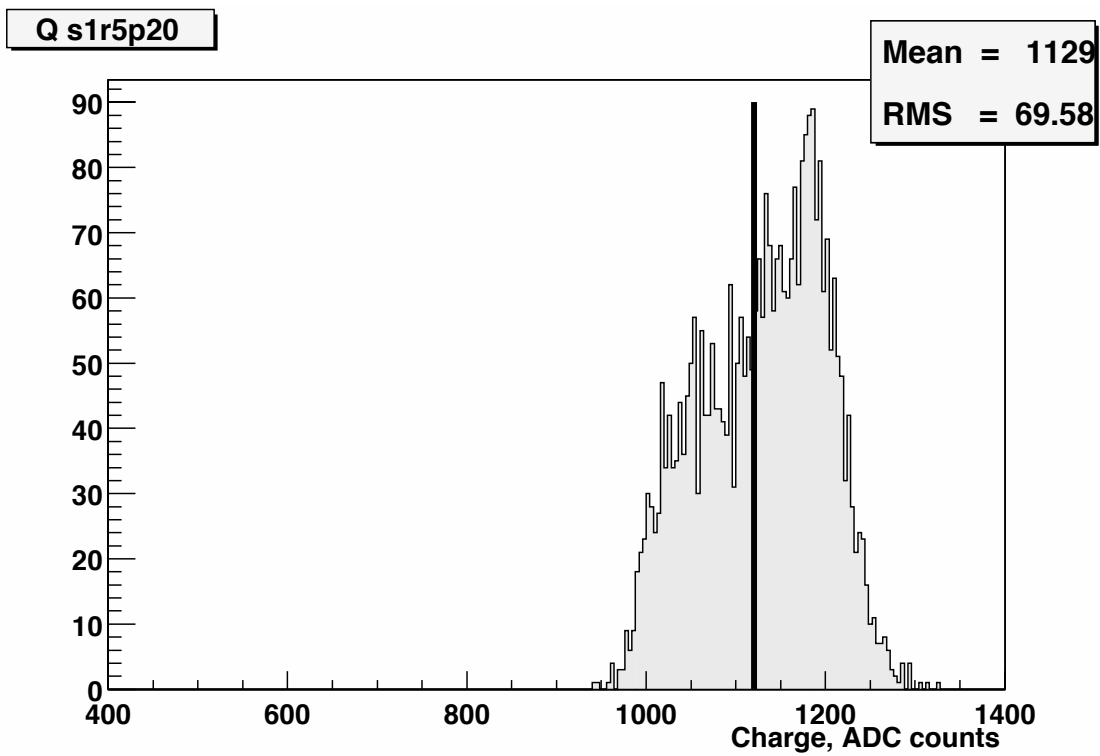
Figure 12: Charges from individual test-charge events as compared to the average charge (top); ratio of individual charges to the average charge (bottom).
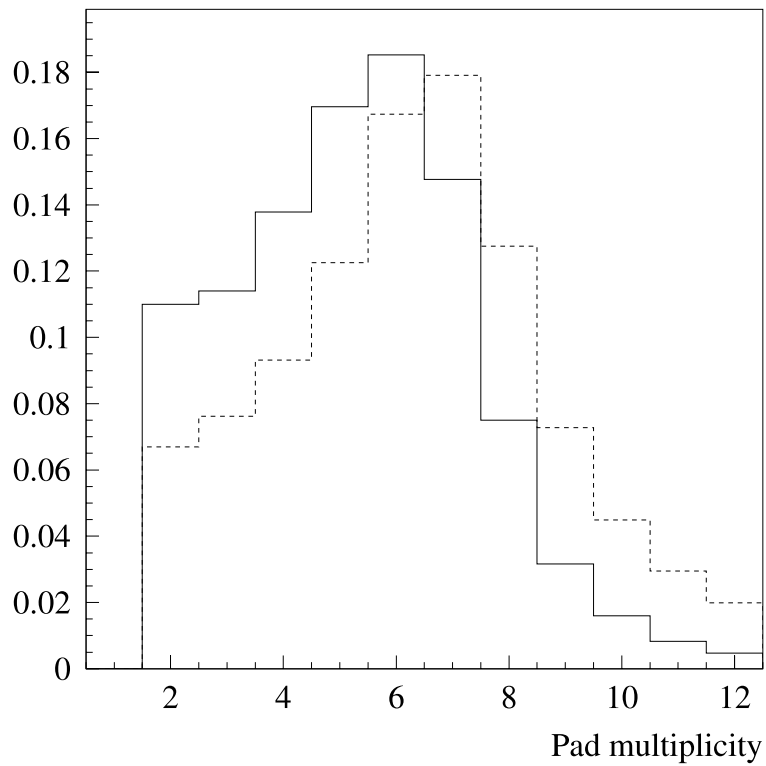
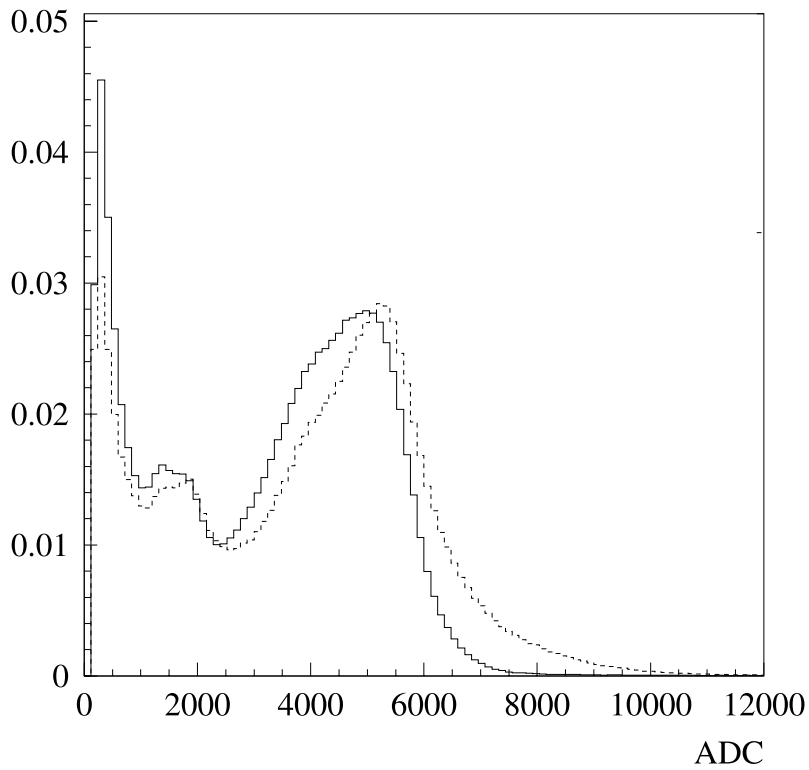Figure 13: Pad multiplicity of krypton clusters before (dashed) and after (full) Xtalk correction.

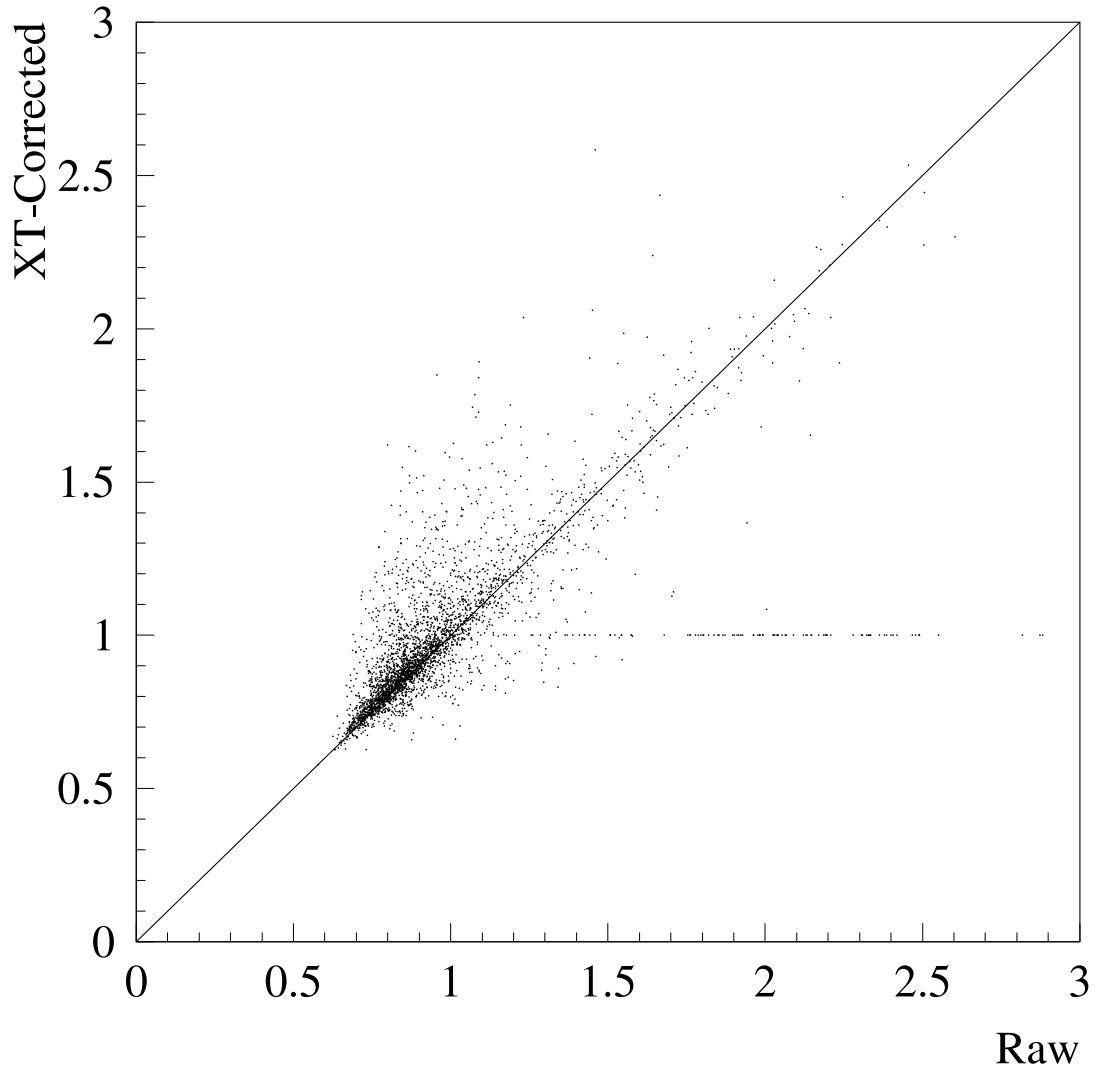Figure 14: Krypton energy spectrum before (dashed) and after (full) Xtalk correction.

Figure 15: Krypton equalization constants before (horizontal) versus after (vertical) Xtalk correction; the average of either set of constants is normalized to unity.
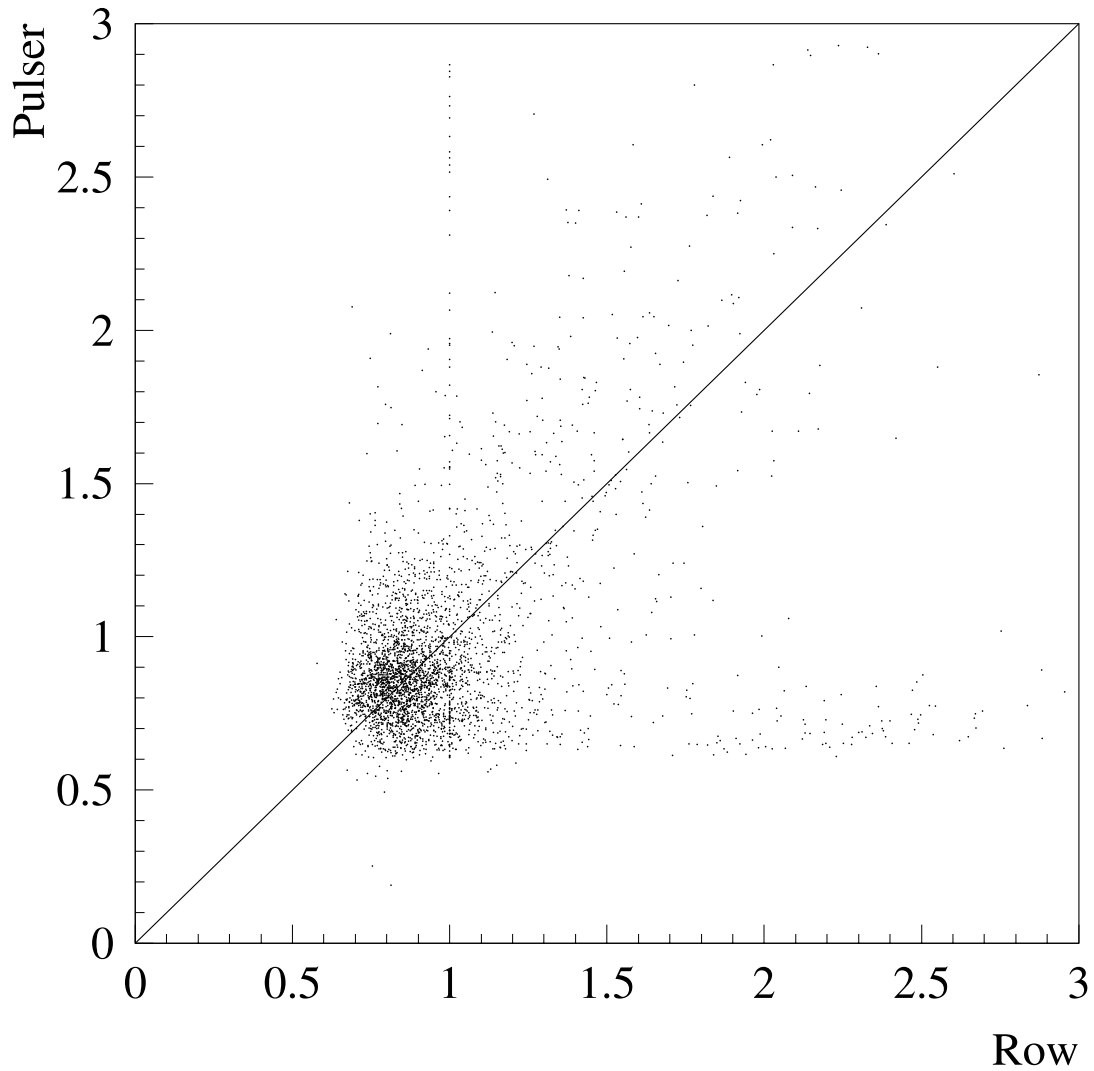
Figure 16: Krypton equalization constants before Xtalk correction (horizontal) versus test-charge equalization constants before Xtalk correction (vertical); the average of either set of constants is normalized to unity.